

We are IntechOpen, the world's leading publisher of Open Access books Built by scientists, for scientists

6,900

Open access books available

185,000

International authors and editors

200M

Downloads

Our authors are among the

154

Countries delivered to

TOP 1%

most cited scientists

12.2%

Contributors from top 500 universities



WEB OF SCIENCE™

Selection of our books indexed in the Book Citation Index
in Web of Science™ Core Collection (BKCI)

Interested in publishing with us?
Contact book.department@intechopen.com

Numbers displayed above are based on latest data collected.
For more information visit www.intechopen.com



Chiral Waves in Graphene Medium and Optical Simulation with Metamaterial

H. Torres-Silva

Additional information is available at the end of the chapter

<http://dx.doi.org/10.5772/51328>

1. Introduction

In modern age Engineers have paved the way for a new generation of faster, more powerful cell phones, computers and other electronics by developing a practical technique to replace silicon with carbon on large surface. The capability of silicon, the material at the heart of computer chips has been harnessed beyond its limits by engineers and carbon has come up as an integrating replacement for the same. The material called "Graphene" which is a single layer of atoms arranged in honeycomb lattice could let electronics to process information and produce radio transmission 10 times better than silicon based devices.

For theorists, such a system is also of great interest because it provides a physical realization of two-dimensional field theories with quantum anomalies. Indeed, the continuum limit of the effective theory describing the electronic transport in graphene is that of two-dimensional massless Dirac fermions. The reported and predicted phenomena include the Klein paradox (the perfect transmission of relativistic particles through high and wide potential barriers), the anomalous quantum Hall effect induced by Berry phases and its corresponding modified Landau levels and the experimental observation of a minimal conductivity.

From the point of view of its electronic properties, graphene is a two-dimensional zero-gap semiconductor with the cone energy spectrum, and its low-energy quasiparticles are formally described by the Dirac-like Hamiltonian [1, 2].

$$H_0 = -i\hbar v_F \sigma \cdot \nabla$$

Where $v_F \approx 10^6 \text{ms}^{-1}$ is the Fermi velocity and $\sigma = (\sigma_x, \sigma_y)$ are the Pauli matrices. The fact that charge carriers are described by the Dirac-like equation, rather than the usual Schrödinger equation, can be seen as a consequence of graphene's crystal structure, which consists of two equivalent carbon sublattices [1, 2]. Quantum mechanical hopping between the sublattices

leads to the formation of two cosine-like energy bands, and their intersection near the edges of the Brillouin zone yields the conical energy spectrum. As a result, quasiparticles in graphene exhibit the linear dispersion relation $E_G = E = \hbar k v_F$, as if they were massless relativistic particles with momentum k (for example, photons) but the role of the speed of light is played here by the Fermi velocity $v_F \approx c/300$. Owing to the linear spectrum, it is expected that graphene's quasiparticles will behave differently from those in conventional metals and semiconductors where the energy spectrum can be approximated by a parabolic (free-electron-like) dispersion relation.

From a crystallographic point of view, the graphene is a triangular Bravais lattice with a diamond-shaped unit tile consisting of two sites so one gets the honeycomb structure. The very unique feature of the graphene band structure is that the two lowest-energy bands, known as the valence and the conduction bands, touch at two isolated points located at the corners of the Brillouin zone. In the immediate vicinity of these degeneracy points, known as the Dirac points, the band structure is a cone. In natural graphene samples, there is exactly one electron per site, and thus, at zero temperature, all levels in the valence band are filled (a situation known as half-filling). As a result, the energy of the last occupied level precisely slices the band structure at the Dirac points. The low-energy excitations of this system are then described by the massless two-dimensional Weyl-Dirac equation and their energy dispersion relation $\omega = v_F k$ is that of relativistic massless fermions with particle-hole symmetry. In graphene these massless fermions propagate with a velocity v_F . The maths is simple but the principles are deep. We will review the formulation of graphene's massless Dirac Hamiltonian, under the chiral electromagnetism approach, like a metamaterial media, hopefully demystifying the material's unusual chiral, relativistic, effective theory. The novel result here is that in our theory we do not make $c \rightarrow v_F$ [1, 2, 27-35], but we obtain v_F as $v_F = c(1 - k_0 T)$ if $k_0 T > 0$ or $v_F = c(1 + k_0 T)$ if $k_0 T < 0$. These results are derived of the Chiral Electrodynamics with T as the chiral parameter and $k_0 = \omega/c$ when the electric wave E is quasi parallel to the magnetic wave H .

With this approach we can review different phenomena such: The Dirac point with a double-cone structure for optical fields, an optical analogy with Dirac fermions in graphene, can be realized in optically homogenous metamaterials. The condition for the realization of Dirac point in optical systems is the varying of refractive index from negative to zero and then to positive.

Also we give a support to the similitude of the band structure of a macroscopic photonic crystal with the electronic band structure of graphene, which is experimentally much more difficult to access, allows the experimental study of various relativistic phenomena. With our analytical and numerical analysis we hope to verify that, similar behaviors exist to electrons in graphene treated as mass-less particle, ie, electron wave propagation.

This chapter presents a short review on the chiral propagation of electron waves in monolayer graphene and optical simulation with optical field in the negative-zero-positive index metamaterial NZPIM and its close connection. Section II presents an enhanced vector diagram of Maxwell's equations for chiral media with quasi parallel electromagnetic fields,

$E \parallel H$. Chiral waves in graphene acting as metamaterial media are discussed in section III. In section IV, two component equations and tunneling rate of Dirac electron in graphene are derived. Section V is about *Zitterbewegung* of optical pulses near the Dirac point inside a negative-zero-positive index metamaterial, and shows that the chiral field near the Dirac point becomes a diffusive wave. The last sections describe the theoretical description of minimal conductivity in graphene under chiral approach and absorption of light by quasi 2D Dirac fermions.

2. A vector diagram of Maxwell's equations for chiral media with $E \parallel H$

The idea of representing Maxwell's time-harmonic equations in homogeneous isotropic media by vector diagram as put forward by Wilton [3] and by S. Uckun [4] deserves consideration. All the common relations between field and potential quantities implied by Maxwell's equations can be represented by a diagram. It is started that the diagram not only illustrates Maxwell's equations, but also many of the methods for constructing diagram are based on the formal similarity between many theorems of vector calculus and those of vector algebra.

An isotropic chiral medium is a macroscopically continuous medium composed of equivalent chiral objects that are uniformly distributed and randomly oriented. A chiral object is a three-dimensional body that cannot be brought into agreement with its mirror image by translation and rotation. An object of this sort has the property of handedness and must be either left-handed or right-handed. An object that is not chiral is said to be achiral, and thus all objects are either chiral or achiral. Due to their novel properties and wide applications in microwave and radar engineering, chiral media has been undergoing extensive research during the last years. That is why this study aims to cover chiral medium for the representation of Maxwell's equations in vector diagram form. In a chiral media a cross coupling between electric and magnetic field exists. Thus, the vector diagram has vectors along all three coordinate axes whereas the vector diagram presented by Wilton [3] for achiral media has vectors only in one plane with H vector normal to it.

2.1. Vector diagram construction

Assuming $\exp(i\omega t)$ time dependence, Maxwell's time-harmonic equations [5, 6] for isotropic, homogeneous, linear media are:

$$\nabla \times \mathbf{E} = -j\omega \mathbf{B} \quad (1)$$

$$\nabla \times \mathbf{H} = j\omega \mathbf{D} + \mathbf{J} \quad (2)$$

$$\nabla \cdot \mathbf{B} = 0 \quad (3)$$

$$\nabla \cdot \mathbf{D} = \rho \quad (4)$$

Chirality is introduced into the theory by defining the following constitutive relations to describe the isotropic chiral medium [5]

$$\mathbf{D} = \varepsilon \mathbf{E} + j\omega \varepsilon T \mathbf{B} \quad (5)$$

$$\mathbf{H} = j\omega \varepsilon T \mathbf{E} + \frac{1 - k_o^2 T^2}{\mu} \mathbf{B} \quad (6)$$

Where the chirality admittance $-j\omega \varepsilon T$ indicates the degree of chirality of the medium, and the ε and μ are permittivity and permeability of the chiral medium, respectively. Since \mathbf{D} and \mathbf{E} are polar vectors and \mathbf{B} and \mathbf{H} are axial vectors, it follows that ε and μ are true scalars and $-j\omega \varepsilon T$ is a pseudoscalar. This means that when the axes of a right-handed Cartesian coordinate system are reversed to form a left-handed Cartesian coordinate system, $-j\omega \varepsilon T$ changes in sign whereas ε and μ remain unchanged.

For a graphical representation of the above relationships, following Wilton's procedure [3], let us assume vector-differential operator, ∇ is an ordinary vector and treat the divergence and curl operations in equations (1) to (4) as ordinary scalar (dot) and vector (cross) products, respectively. Equation (3) implies that ∇ is perpendicular to \mathbf{B} and the vector $\nabla \times \mathbf{B}$ must be perpendicular to both ∇ and \mathbf{B} .

As shown in Figure 1, three transverse coordinate axes are chosen as ∇ , from Equation (1) $\mathbf{B} = -\nabla \times \mathbf{E} / (j\omega)$ and, $\nabla \times \mathbf{B} / (j\omega \varepsilon \mu) = \nabla \times \nabla \times \mathbf{E} / k^2$ where $k^2 = \omega^2 \varepsilon \mu$.

Since $\nabla \cdot \mathbf{B} = 0$ always, this conditions will hold identically if \mathbf{B} is expressed as the curl of a vector potential \mathbf{A} since the divergence of the curl of a vector is identically zero, thus

$$\mathbf{B} = \nabla \times \mathbf{A} \quad (7)$$

and \mathbf{A} must be perpendicular to both ∇ and \mathbf{B} and lie in ∇ and $\nabla \times \mathbf{B}$ plane. However, \mathbf{A} is not unique since only its components perpendicular to ∇ contribute to the cross product. Therefore, $\nabla \cdot \mathbf{A}$, the component of \mathbf{A} parallel to ∇ , must be specified. The curl equation for \mathbf{E} , as in Equation (1), and Equation (7) give $\nabla \times (\mathbf{E} + j\omega \mathbf{A}) = 0$ where the quantity in parentheses should be parallel to ∇ and the curl of the gradient of a scalar function ϕ is identically zero; so the above equation is $\mathbf{E} + j\omega \mathbf{A} = -\nabla \phi$ or

$$\mathbf{E} = -j\omega \mathbf{A} - \nabla \phi \quad (8)$$

That is shown in Figure 1.

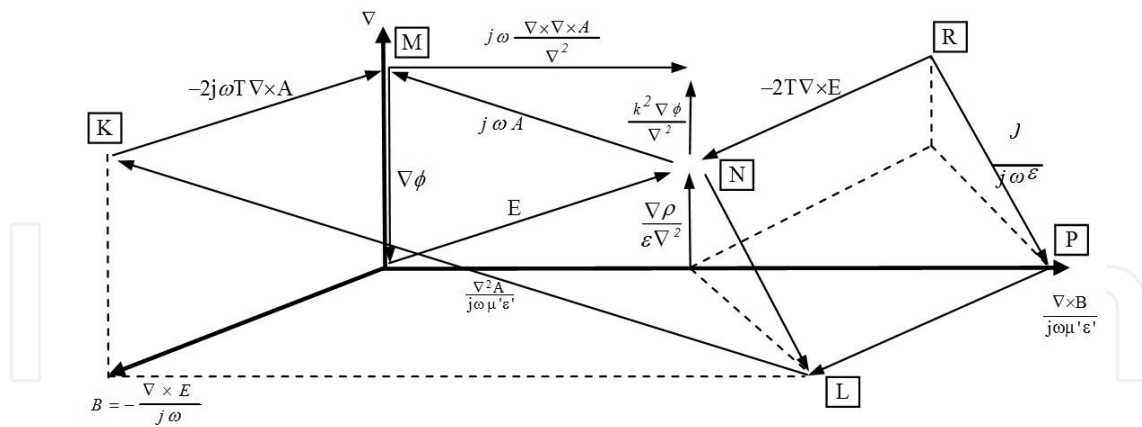


Figure 1. Diagram of the full Maxwell System for a chiral media with Lorentz gauge $\frac{\mu\epsilon}{1-k_0^2 T^2} = \mu' \epsilon'$.

Following the Uckun's approach [5], we substitute Equation (7) into Equation (6) having

$$\mathbf{H} = \frac{1-k_0^2 T^2}{\mu} \nabla \times \mathbf{A} + j\omega\epsilon T \mathbf{E} \tag{9}$$

Substituting Equation (9) and Equation (5) into Equation (2) gives

$$\nabla \times \nabla \times \mathbf{A} + j \frac{\omega\mu\epsilon T}{1-k_0^2 T^2} \nabla \times \mathbf{E} = j \frac{\omega\mu\epsilon}{1-k_0^2 T^2} \mathbf{E} - \frac{\omega^2\mu\epsilon T}{1-k_0^2 T^2} \mathbf{B} + \frac{\mu}{1-k_0^2 T^2} \mathbf{J}$$

$$\nabla \times \nabla \times \mathbf{A} + j \frac{\omega\mu\epsilon T}{1-k_0^2 T^2} \nabla \times \mathbf{E} = j \frac{\omega\mu\epsilon}{1-k_0^2 T^2} \mathbf{E} - \frac{\omega^2\mu\epsilon T}{1-k_0^2 T^2} \mathbf{B} + \frac{\mu}{1-k_0^2 T^2} \mathbf{J},$$

playing the value of $\nabla \times \mathbf{E}$ from Equation (1) into the above equation $\nabla \times \nabla \times \mathbf{A} + 2 \frac{\mu\omega^2\epsilon T}{1-k_0^2 T^2} \mathbf{B} = j \frac{\omega\mu\epsilon}{1-k_0^2 T^2} \mathbf{E} + \frac{\mu}{1-k_0^2 T^2} \mathbf{J}$ and using

the vector identity $\nabla \times \nabla \times \mathbf{A} = \nabla(\nabla \cdot \mathbf{A}) - \nabla^2 \mathbf{A}$ enables us to write the above equation as

$$\nabla^2 \mathbf{A} + 2 \frac{\omega^2\mu\epsilon T}{1-k_0^2 T^2} \nabla \times \mathbf{A} = \nabla(\nabla \cdot \mathbf{A}) - j \frac{\omega\mu\epsilon}{1-k_0^2 T^2} \mathbf{E} - \frac{\mu}{1-k_0^2 T^2} \mathbf{J}$$

$$\nabla^2 \mathbf{A} + 2 \frac{\omega^2\mu\epsilon T}{1-k_0^2 T^2} \nabla \times \mathbf{A} = \nabla(\nabla \cdot \mathbf{A}) - j \frac{\omega\mu\epsilon}{1-k_0^2 T^2} \mathbf{E} - \frac{\mu}{1-k_0^2 T^2} \mathbf{J},$$

so using Equation (8), we have

$$\nabla^2 \mathbf{A} + \frac{k_0^2}{1-k_0^2 T^2} \mathbf{A} + 2 \frac{\omega^2\mu\epsilon T}{1-k_0^2 T^2} (\nabla \times \mathbf{A}) = \nabla(\nabla \cdot \mathbf{A} - j \frac{\omega^2\mu\epsilon T\phi}{1-k_0^2 T^2}) - \frac{\mu}{1-k_0^2 T^2} \mathbf{J} \tag{10}$$

Here $\nabla \cdot \mathbf{A}$ is arbitrary, so in order to specify $\nabla \cdot \mathbf{A}$, for unique \mathbf{A} , we may choose

$$\nabla \cdot \mathbf{A} = j \frac{\omega\mu\epsilon\phi}{1-k_0^2 T^2} \tag{11}$$

And eliminate the term in parentheses in Equation (10). The choice in Equation (11) can be known as a chiral Lorentz gauge. Then Equation (10) will be simplified to

$$\nabla^2 \mathbf{A} + \frac{k_0^2}{1-k_0^2 T^2} \mathbf{A} + 2 \frac{\omega^2 \mu \varepsilon T}{1-k_0^2 T^2} (\nabla \times \mathbf{A}) = - \frac{\mu}{1-k_0^2 T^2} \mathbf{J} \quad (12)$$

Divide both sides of Equation (12) by $(j \frac{\omega \mu \varepsilon}{1-k_0^2 T^2})$ and reorganize it to get

$$(1-k_0^2 T^2) \frac{\nabla^2 \mathbf{A}}{j \omega \mu \varepsilon} = j \omega \mathbf{A} + 2 j \omega T (\nabla \times \mathbf{A}) - \frac{1}{j \omega \varepsilon} \mathbf{J} \quad (13)$$

(Figure 1, shows this vectorial equation).

The difference between our approach and the Uckun's procedure [4], is that we take the chiral media characterized by $\mathbf{D} = \varepsilon(\mathbf{E} + T \nabla \times \mathbf{E})$ and $\mathbf{B} = \mu(\mathbf{H} + T \nabla \times \mathbf{H})$. In this form we can obtain the condition of quasi spatial parallel condition between \mathbf{B} and \mathbf{E} where the main equation is like a Beltrami equation which is important for the numerical simulation of graphene systems.

Placing the value of \mathbf{B} from Equation (1) into Equation (5) $\mathbf{D} = \varepsilon(\mathbf{E} + T \nabla \times \mathbf{E})$ will be obtained. Placing the value of \mathbf{H} , from Equation (6), and \mathbf{D} into Equation (2) will give

$$\nabla \times (j \omega \varepsilon T \mathbf{E} + \frac{1-k_0^2 T^2}{\mu} \mathbf{B}) = j \omega (\varepsilon \mathbf{E} + \varepsilon T \nabla \times \mathbf{E}) + \mathbf{J}$$

by rearranging this equation we obtain

$$(1-k_0^2 T^2) \frac{\nabla \times \mathbf{B}}{j \omega \mu \varepsilon} = \mathbf{E} + 2 T \nabla \times \mathbf{E} + \frac{\mathbf{J}}{j \omega \varepsilon} \quad (14)$$

will be obtained as shown in Figure 1. In this figure we put $\mu \rightarrow \mu / (1-k_0^2 T^2)$.

Taking divergence of Equation (5) and using Equations (3) and (4) in it

$$\rho = \varepsilon \nabla \cdot \mathbf{E} \quad (15)$$

will be derived. To find the projection of \mathbf{E} onto ∇ , from Equation(15) $\nabla \cdot \mathbf{E} = \rho / \varepsilon$, take the gradient of both sides and divide by scalar value ∇^2 to normalize ∇ to a unit vector. So

$$\frac{\nabla (\nabla \cdot \mathbf{E})}{\nabla^2} = \frac{\nabla \rho}{\varepsilon \nabla^2} \quad (16)$$

Similarly, getting gradient of both sides of Equation(11), using the vector identify $\nabla \times \nabla \times \mathbf{A} + \nabla^2 \mathbf{A}$ for $\nabla (\nabla \cdot \mathbf{A})$ and normalizing by ∇^2 we have:

$$j \omega \frac{\nabla \times \nabla \times \mathbf{A}}{\nabla^2} + j \omega \mathbf{A} = k^2 \frac{\nabla \phi}{\nabla^2} \quad (17)$$

So it will be obtained as parallel component of \mathbf{A} to ∇ coordinate.

By using Equations (8), (13), (14), (16), and (17) the vector diagram of Lorenz gauge can be completed as shown in Figure 1, where all Maxwell's relations and potential quantities appear.

Now let us examine derivation of some relations from the diagram. For example, it is seen that the component of \mathbf{E} and $\mathbf{J}/(j\omega\epsilon)$ parallel to ∇ must be equal and opposite. By taking the divergence of Equation (14) and using $\nabla \cdot \mathbf{E} = \rho/\epsilon$ can be shown that

$$\nabla \cdot \mathbf{E} = -\frac{1}{j\omega\epsilon} \nabla \cdot \mathbf{J} = \frac{\rho}{\epsilon} \quad (18)$$

Taking the gradient in both sides of Equation (18) and dividing it by scalar value ∇^2 will give the same value as Equation (16) with opposite sign. From the right side of Equation (18) it is seen that

$$\rho = -\frac{1}{j\omega} \nabla \cdot \mathbf{J} \quad (19)$$

This is the known continuity equation. Since the divergence of the curl of any vector is identically zero, the divergence of Equation (2) yields $0 = j\omega \nabla \cdot \mathbf{D} + \nabla \cdot \mathbf{J}$. Using Equation (4) convert this immediately into continuity equation as, expected. Again, as seen in Figure 1, $2T \nabla \times \mathbf{E}$ and $-j\omega 2T \nabla \times \mathbf{A}$ are equal and opposite vectors. From Equation (8), taking curl of both side and using the vector identity $\nabla \times \nabla \phi = 0$ will show that

$$2T \nabla \times \mathbf{E} = -j\omega 2T \nabla \times \mathbf{A} \quad (20)$$

as expected. By using the vector calculus a few possible equations from the vector diagram can be written as follows

$$2T \nabla \times \mathbf{E} + \frac{\mathbf{J}}{j\omega\epsilon} - (1 - k_o^2 T^2) \frac{\nabla \times \mathbf{B}}{j\omega\mu\epsilon} - \nabla \phi - j\omega \mathbf{A} = 0 \quad (21)$$

$$j\omega \frac{\nabla \times \nabla \times \mathbf{A}}{\nabla^2} - k^2 \frac{\nabla \phi}{\nabla^2} - \mathbf{E} - \nabla \phi = 0 \quad (22)$$

$$j\omega \frac{\nabla \times \nabla \times \mathbf{A}}{\nabla^2} - k^2 \frac{\nabla \phi}{\nabla^2} + \frac{\mathbf{J}}{j\omega\epsilon} + (1 - k_o^2 T^2) \frac{\nabla^2 \mathbf{A}}{j\omega\mu\epsilon} - 2j\omega T \nabla \times \mathbf{A} = 0 \quad (23)$$

$$(1 - k_o^2 T^2) \frac{\nabla^2 \mathbf{A}}{j\omega\mu\epsilon} - 2j\omega\beta \nabla \times \mathbf{A} + \nabla \phi + (1 - k_o^2 T^2) \frac{\nabla \times \mathbf{B}}{j\omega\mu\epsilon} - 2T \nabla \times \mathbf{E} = 0 \quad (24)$$

For example, adding Equations (13) and (14) side by side and using Equation (8) will give Equation (24) which shows the correctness of the equation derived from the diagram 1. Instead of Lorenz gauge we can choose Coulomb's gauge.

$$\nabla \cdot \mathbf{A}_c = 0 \quad (25)$$

In Equation (10) so that it will take the form

$$\nabla^2 \mathbf{A}_c + k^2 \mathbf{A}_c - 2 \frac{\omega^2 \mu \epsilon T}{1 - k_o^2 T^2} (\nabla \times \mathbf{A}_c) = j \frac{\omega \mu \epsilon}{1 - k_o^2 T^2} \nabla \phi - \frac{\mu}{1 - k_o^2 T^2} \mathbf{J}$$

where the subscript "c" is used it indicate Coulomb's gauge. Using Equation (8) and (20) in the above equation

$$-(1 - k_o^2 T^2) \frac{\nabla^2 \mathbf{A}_c}{j \omega \mu \epsilon} - 2T \nabla \times \mathbf{E} = \mathbf{E} + \frac{\mathbf{J}}{j \omega \epsilon} \quad (26)$$

will be obtained. Placing the values of Equations (5) and (6) into Equation (2) will give

$$\nabla \times (j \omega \epsilon T \mathbf{E} + \frac{(1 - k_o^2 T^2)}{\mu} \mathbf{B}) = j \omega (\epsilon \mathbf{E} + j \omega \epsilon T \mathbf{B}) + \mathbf{J}$$

and value of $\nabla \times \mathbf{E}$ from Equation (1) will give

$$(1 - k_o^2 T^2) \frac{\nabla \times \mathbf{B}}{j \omega \mu \epsilon} + 2 j \omega T \mathbf{B} = \mathbf{E} + \frac{\mathbf{J}}{j \omega \epsilon} \quad (31)$$

.

Combining these equations with Equation (26) and using Equation (7) we have

$$(1 - k_o^2 T^2) \frac{\nabla \times \mathbf{B}}{j \omega \mu \epsilon} = -(1 - k_o^2 T^2) \frac{\nabla^2 \mathbf{A}_c}{j \omega \mu \epsilon} \quad (27)$$

By using the same coordinates axes ∇ , \mathbf{B} and $(1 - k_o^2 T^2) \nabla \times \mathbf{B} / (j \omega \mu \epsilon)$ and Equation (1), (8), (16), (26) and (27) for the Coulomb gauge. It is clear from Equation (25) that the component of the vector \mathbf{A} parallel to ∇ is equal to zero.

As seen in Figure 1, Lorenz gauge are the best choice because these make \mathbf{A} either parallel or perpendicular to any of the other vectors and simplify its relationship to those vectors. In Figure 1a, if the chirality factor T , goes to zero, point K , L and R approach point M , P , and N respectively, in which case the diagram will be the same as in Reference [3] for linear, homogeneous, isotropic achiral medium. If $(1 - k_o^2 T^2) \rightarrow 0$ then \mathbf{E} is quasi parallel to \mathbf{B} , and parallel to \mathbf{A} . Also all vectors remain in an only plane. (see Figure 2).

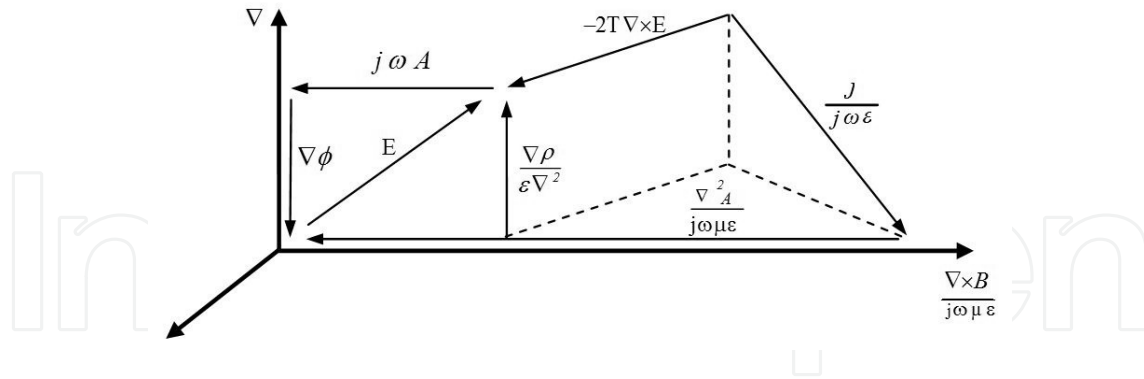


Figure 2. Two dimensional condition when $(1 - k_0^2 T^2) \rightarrow 0$ for a graphene system, the thickness is about one carbon atom

This Beltrami condition is useful to numerical calculations in graphene. We apply this approach to a two dimensional chiral graphene slab. This result cannot be obtained with the Uckun's approach [4]. In terms of chiral magnetic potential A_c with $J = 0$, and $\nabla \rho = 0$ we have the wave equation

$$\nabla^2 A_c + \frac{k_0^2}{1 - k_0^2 T^2} A_c + 2 \frac{\omega^2 \mu \epsilon T}{1 - k_0^2 T^2} (\nabla \times A_c) = 0 \quad (28)$$

As $k = \sqrt{k_x^2 + k_y^2 + k_z^2}$, if $k_x = k \sin \theta$, $k_y = 0$, and $k_z = k \cos \theta$, we have the matrix:

$$\begin{pmatrix} -k^2(1 - k_0^2 T^2) + k_0^2 & -2jk_0^2 k T \cos \theta & 0 \\ 2jk_0^2 k T \cos \theta & -k^2(1 - k_0^2 T^2) + k_0^2 & -2jk_0^2 k T \sin \theta \\ 0 & 2jk_0^2 k T \sin \theta & -k^2(1 - k_0^2 T^2) + k_0^2 \end{pmatrix} \begin{pmatrix} A_x \\ A_y \\ A_z \end{pmatrix} = 0 \quad (29)$$

The dispersion relation of the transversal wave is $(-k^2(1 - k_0^2 T^2) + k_0^2)^2 - 4k_0^4 k^2 T^2 (\sin^2 \theta + \cos^2 \theta) = 0 \Rightarrow k = k_{\pm} = \pm k_0 / (1 \pm k_0 T)$.

That is

$$k_{\pm} = \pm k_0 / (1 \pm k_0 T) = \pm \frac{\omega}{c} (1 \pm k_0 T)^{-1} \quad (30)$$

So we have $k_{\pm} = \pm \frac{\omega}{c} (1 \pm k_0 T)^{-1} = \omega / v_F$ with $v_F = c(1 \pm k_0 T)$ if we consider a bi dimensional graphene system.

The novel result here is that in our chiral theory we do not make $c \rightarrow v_F$ but we obtain v_F as $v_F = c(1 - k_0 T)$ if $k_0 T > 0$ or $v_F = c(1 + k_0 T)$ if $k_0 T < 0$. These results are derived of the Chiral Elec-

trodynamicity with T as the chiral parameter and $k_0 = \omega / c$ [5, 6, 7]. This situation corresponds to a model of chiral electron where the E field is almost parallel to the H field, the movement of electrons is helical in the valence band of the membrane graphene. Semi classically, for a hydrogen atom, this condition was shown by Huang [36] for E wave perpendicular to H wave with radiation and by Torres-Silva for E parallel to H , without radiation. See refs ([5, 37, 38]). Here, we extend this result to the electron bound to carbon atom.

In the next section we study the situation when the refractive index is negative.

3. Chiral waves in graphene acting as metamaterial media

Metamaterials are composite materials in which both permittivity and permeability possess negative values at some frequencies has recently gained considerable attention [see e.g., [8-12]. This idea was originally initiated by Veselago in 1967, who theoretically studied plane wave propagation in a material whose permittivity and permeability were assumed to be simultaneously negative [11]. Recently Shelby, Smith, and Schultz constructed such a composite medium for the microwave regime, and experimentally showed the presence of anomalous refraction in this medium [10]. Previous theoretical study of electromagnetic wave interaction with omega media using the circuit-model approach had also revealed the possibility of having negative permittivity and permeability in omega media for certain range of frequencies [9].

The anomalous refraction at the boundary of such a medium with a conventional medium, and the fact that for a time-harmonic monochromatic plane wave the direction of the Poynting vector is antiparallel with the direction of phase velocity, can lead to exciting features that can be advantageous in design of novel devices and components. For instance, as a potential application of this material, compact cavity resonators in which a combination of a slab of conventional material and a slab of metamaterial with negative permittivity and permeability are possible. The problems of radiation, scattering, and guidance of electromagnetic waves in metamaterials with negative permittivity and permeability, and in media in which the combined paired layers of such media together with the conventional media are present, can possess very interesting features leading to various ideas for future potential applications such as phase conjugators, unconventional guided-wave structures, compact thin cavities, thin absorbing layers, high-impedance surfaces, to name a few. In this section, we will first present a brief overview of electromagnetic properties of the media with negative permittivity and permeability, and we will then discuss some ideas for potential applications of these materials.

Such a medium is therefore termed left-handed medium [12]. In addition to this "left-handed" characteristic, there are a number of other dramatically different propagation characteristics stemming from a simultaneous change of the signs of ϵ and μ , including reversal of both the Doppler shift and the Cerenkov radiation, anomalous refraction, and even reversal of radiation pressure to radiation tension. This configuration exhibit also chirality and a rotation of the polarization so the analysis of metamaterial presented by several authors pro-

vides a good but not exact characterization of the metamaterial [9]. The evidence of chirality behavior suggests that if it is included in the conditions to obtain a metamaterial behavior of a medium further progress will be obtained. In this short paper, we propose to investigate the conditions to obtain a metamaterial having simultaneously negative ϵ and negative μ and very low eddy current loss. As a initial point, we consider a media where the electric polarization depends not only on the electric field E , and the magnetization depends not only on the magnetic field H , and we may have, for example, constitutive relations given by the Born-Federov formalism [12].

$$D(\vec{r}, \omega) = \epsilon(\omega)(E(\vec{r}, \omega) + T(\omega)\nabla \times E(\vec{r}, \omega)) \quad (31)$$

$$B(\vec{r}, \omega) = \mu(\omega)(H(\vec{r}, \omega) + T(\omega)\nabla \times H(\vec{r}, \omega)) \quad (32)$$

The pseudoscalar T represents the chirality of the material and it has length units. In the limit $T \rightarrow 0$, the constitutive relations (31) and (32) for a standard linear isotropic lossless dielectric with permittivity ϵ and permeability μ are recovered.

According to Maxwell's equations, electromagnetic waves propagating in a homogeneous dielectric magnetic material are either positive or negative transverse circularly polarized waves, and can be expressed as

$$E^\pm(\vec{r}, t) = \hat{E}_0^{(\pm)} e^{-j(k_\pm z - \omega_0 t)} \quad (33)$$

$$H^\pm(\vec{r}, t) = \hat{H}_0^{(\pm)} e^{-j(k_\pm z - \omega_0 t)} \quad (34)$$

where $E_0^\pm = E_0(\hat{x} \pm i\hat{y})$, and $\nabla \times \vec{E}^\pm(\vec{r}, t) = \mp k_\pm \vec{E}^\pm$, $k_\pm \geq 0$ is the chiral wave number.

If the phase velocity and energy flow are in the same directions, and from Maxwell's equation, one can see that the electric E and magnetic field H and the wave vector k will form a right-handed triplet of vectors. This is the usual case for right-handed materials. In contrast, if the phase velocity and energy flow are in opposite directions, and E , H , and k will form a left-handed triplet of vectors. This is just the peculiar case for left handed materials where the effective permittivity $\epsilon(1 + T\nabla \times)$ and the effective permeability $\mu(1 + T\nabla \times)$ are simultaneously negative. So, for incident waves of a given frequency ω , we can determine whether wave propagation in the composite is right handed or left handed through the relative sign changes of k .

To advance in our propose we consider other more popular representation to describe a chiral medium, [12] as

$$D = \epsilon_p E + (\chi + i\kappa)H, \quad (35)$$

$$B = \mu_p H + (\chi - i\kappa)E, \quad (36)$$

in which electromagnetic coupling terms are added to the basic terms. Bi-isotropy or bianisotropy is used for calling such constitutive equations, according to the parameters to be scalars or tensors. If $\kappa=0$ and $\chi \neq 0$, it is the Tellegen medium; if $\kappa \neq 0$ and $\chi=0$, as the requirement of reciprocity, it is the Pasteur medium:

$$\mathbf{D} = \varepsilon_p \mathbf{E} + i\kappa \mathbf{H}, \quad (37)$$

$$\mathbf{B} = \mu_p \mathbf{H} + i\kappa \mathbf{E}, \quad (38)$$

There is a long dispute on strong chiral medium since it was introduced theoretically. Traditional electromagnetic conclusions have limited us to understand strong chirality, i.e. $k_+ T \geq 1$ or $\mu_p \varepsilon_p \kappa^2$, until we see the fact that artificial Veselago's medium [9] was successfully realized in certain frequency bands [3]. For the case, $E \parallel \mathbf{H}$, we have to ask the following question: can strong chiral medium exist?

In Ref. [14], the reason for traditional restriction of chirality parameters was concluded

as: 1) The wave vector of one eigenwave will be negative; 2) The requirement of a positive definite matrix to keep positive energy:

$$\begin{pmatrix} \varepsilon_p & i\kappa \\ -i\kappa & \mu_p \end{pmatrix} \quad (39)$$

With the exploration of backward-wave medium, we know that negative wave vector, or opposite phase and group velocities, are actually realizable. And there is an unfortunate mathematical error in the second reason: in linear algebra, only if it is real and symmetric, positive definite matrix is equivalent to that all eigenvalues should be positive. The matrix (14) is a complex one, making the analysis on restriction of positive energy meaningless.

Actually, in a strong bi-isotropic medium with constitutive relations as Eqs. (1) and (2), the energy can be drawn as

$$w = w_e + w_m = \frac{\mathbf{D} \cdot \mathbf{E}}{2} + \frac{\mathbf{B} \cdot \mathbf{H}}{2} = \varepsilon \frac{|\mathbf{E}|^2}{2} + \mu \frac{|\mathbf{H}|^2}{2} \quad (40)$$

Mathematically, the amount of energy density propagated is proportional to the magnitude of the Poynting vector \vec{S} , where $\mathbf{S} = \mathbf{E} \times \mathbf{H}$. With the condition $E \parallel \mathbf{H}$, $S(r, t) = 0$ so we find right circularly polarized wave or left circularly polarized wave.

The concept of parallel fields is important in the theoretical formulation of: Space electromagnetism and vacuum, the classical and quantum gravitational fields, the study of elementary particles, operator and Dirac matrices, fields and chiral electrodynamics [15, 16]. If we

put $E = \alpha B$ and solving the Maxwell equations with the Born Fedorov relations we find $\alpha = i / \sqrt{\mu \epsilon / 4}$ $E = i \eta H = i \sqrt{\frac{\mu / 2}{\epsilon / 2}} H$ so $\epsilon(\omega)$, $\mu(\omega)$ and T are transformed as:

$$\epsilon_{\parallel} = \frac{\epsilon}{2} = \epsilon_p \left(1 - \frac{\kappa^2}{\mu_p \epsilon_p} \right) \quad (41)$$

$$\mu_{\parallel} = \frac{\mu}{2} = \mu_p \left(1 - \frac{\kappa^2}{\mu_p \epsilon_p} \right) \quad (42)$$

$$T = \frac{\kappa}{\omega(\mu_p \epsilon_p - \kappa^2)} \quad (43)$$

In this case the total density energy is may be

$$w = w_e + w_m = 0 \quad (44)$$

In this special case where the energy propagated in one direction is equal to that propagated in the opposite direction, there is no net energy flow in the medium and the sum of the two TEM waves form what is generally known as a standing wave. The condition for a standing wave is that the time average of S vanishes. This can be achieved if S is zero all the time everywhere in the region of space under consideration, i.e., $S(r, t) = 0$ (see Fig. 4). Examination of Eq. (39) shows that $S = 0$ if $E \parallel H$. In this last case, a particular solution of Eq. (31,3 2) is when $k_0^2 T^2 = 1$, where we have the condition $E \parallel H$, and $E = i \eta H$, so we find the Beltrami force free equation $E + 2T \nabla \times E = 0$ and the vector Poynting $S(r, t)$ vanishes [15-16].

In terms of Eqs. (41-42), if $\mu_p \epsilon_p < \kappa^2$ for whole frequency range, the energy will still keep positive as long as the permittivity and permeability are positive, under the weak spatial dispersion condition. Therefore, the real reason for traditional strong-chirality limitation is neither negative wave vector nor energy conversation. Next we will point out two other important reasons.

First, with the assumption that $\epsilon_p > 0$, $\mu_p > 0$, $\kappa > 0$ and $\kappa > \sqrt{\mu_p \epsilon_p}$, we easily show that ϵ_{\parallel} , μ_{\parallel} and T turn to negative from the transformation between Pasteur constitutive relations and BF relations shown in Eqs. (41)-(43). This is absolutely unacceptable before people realizing Veselago's medium. Actually, strong chiral medium can be equivalent to Veselago's medium for the right circularly polarized wave [9-16]. The negative ϵ and μ have shown such a point. Hence the negative sign in the BF model is not strange at all, since we realize effective double-negative with strong chirality parameter instead of simultaneously frequency resonances. For a limiting case, the chiral nihility [10], in which $\mu_p \rightarrow 0$ and $\epsilon_p \rightarrow 0$ while $\kappa \neq 0$, the parameters in DBF representation become $\epsilon_{\parallel} \rightarrow \infty$, $\mu_{\parallel} \rightarrow \infty$ and $T = -1 / \omega \kappa$, remaining a finite value after a simple mathematical analysis. There is no evidence that strong chirality cannot exist in this aspect.

Second, it is the effectiveness of linear models. Similar to the case that linear optical and electromagnetic models can no longer deal with very strong optical intensity and electromagnetic field, we introduce nonlinear optics to take into account the higher order terms of polarization.

If the spatial dispersion is strong enough, the higher order coupling terms cannot be neglected as before. People used to mistake strong chirality with strong spatial dispersion, hence adding a limitation to chirality parameter, $\kappa\sqrt{\mu_p\epsilon_p}$. We believe that this is the most probable reason.

However, the strong spatial dispersion is embodied in the BF model, e.g. the value of T , while the strong chirality is represented by the Pasteur model, e.g. the ratio of κ to $\sqrt{\mu_p\epsilon_p}$. That is to say, strong chirality does not necessarily lead to strong spatial dispersion.

Based on Eqs. (41)-(43), we have computed T and $\epsilon_{\parallel}/\epsilon_p$ or μ_{\parallel}/μ_p versus $\kappa/\sqrt{\mu_p\epsilon_p}$, as shown in Figs. 2 and 3. When κ is very close to $\sqrt{\mu_p\epsilon_p}$, the value of T is quite large, indicating a strong spatial dispersion. Hence the singular point is the very point of traditional limitation. However, with κ continuously increasing, the spatial dispersion strength falls down very quickly. Therefore, if κ is not around $\sqrt{\mu_p\epsilon_p}$, e.g. $\kappa < 0.8\sqrt{\mu_p\epsilon_p}$ or $\kappa > 1.2\sqrt{\mu_p\epsilon_p}$, we need not take nonlinear terms into consideration at all. Hence the strong spatial dispersion and nonlinearity cannot put the upper limitation to chirality parameters either.

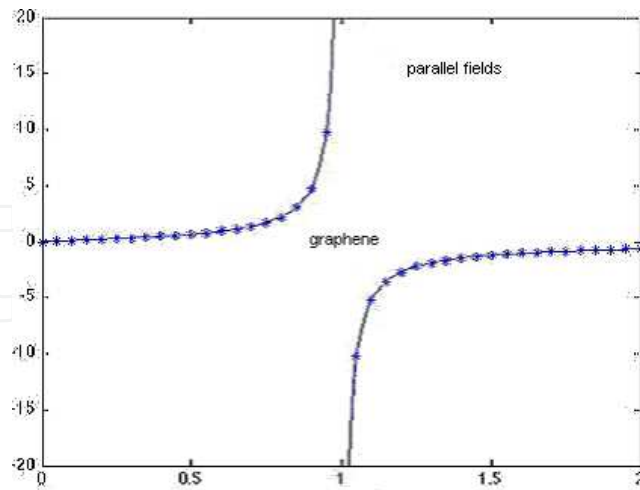


Figure 3. The strength relationship of chirality and spatial dispersion. $\omega T / c$ versus $\kappa / \sqrt{\mu_p\epsilon_p}$. The point of $\kappa / \sqrt{\mu_p\epsilon_p} = 1$ is singularity, corresponding infinite spatial dispersion coefficient T . When $\kappa / \sqrt{\mu_p\epsilon_p} > 1$, T becomes negative for keeping the positive rotation term coefficients with negative μ_{\parallel} and ϵ_{\parallel} . The 2-D grapheme system may be modeled when $\omega T / c \sim 0.9 - 1.1$ and $\kappa / \sqrt{\mu_p\epsilon_p} \sim 1$

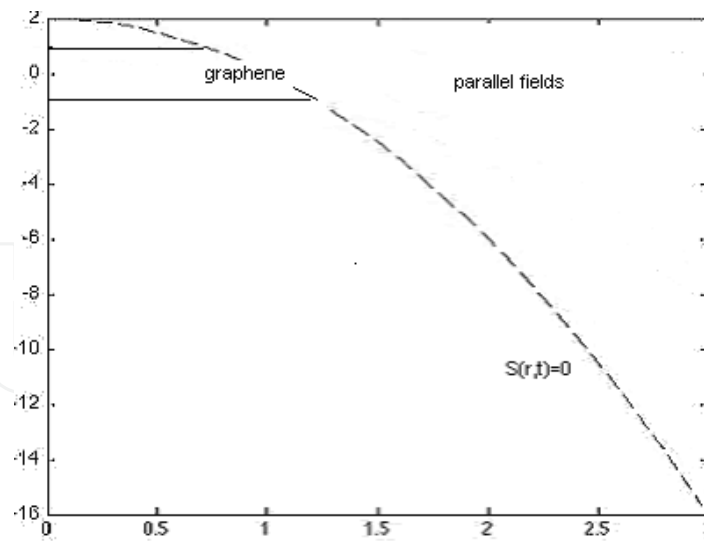


Figure 4. $\epsilon_{||} / \epsilon_p, \mu_{||} / \mu_p$ versus $k / \sqrt{\mu_p \epsilon_p}$. With chirality strength increases, $\epsilon_{||}$ and $\mu_{||}$ reduces quickly from ϵ_p and μ_p to $-\infty$. The case 2-D graphene corresponds to $k / \sqrt{\mu_p \epsilon_p} \sim 1$.

If $\omega |T| / c = 0.9927$ or $\omega |T| / c = 1.0073$, we have that the Fermi velocity is given by $v_F = c(1 \pm k_0 T)$, so it appears a connection between the chiral electrodynamics and the fine structure constant.

From Figure 4. we see that near of $\epsilon_{||} / \epsilon_p, \mu_{||} / \mu_p \approx 0$ the graphene have a linear behavior so the Beltrami equation is

$$\nabla \times \vec{E}^{\pm}(\vec{r}, t) = \mp k_{\pm} \vec{E}^{\pm} \tag{50}$$

Solving Beltrami's equation with boundary conditions, we can demonstrate the optical *Zitterbewegung* effect by means of electromagnetic pulses propagating through a negative-zero-positive index metamaterial (NZPIM) if we make

$$k_{\pm} = \mp k_0 / (1 \pm k_0 T) = \mp \omega / v_F \text{ with}$$

$$v_F = c(1 \pm k_0 T) \tag{51}$$

Thus in optics, the Beltrami's equation for electromagnetic waves can be reduced to the Helmholtz equation.

In later sections we discuss some effects such as *Zitterbewegung* of optical pulses, diffusion phenomenon and tunneling rate of dirac electron in graphene.

4. Two component equations and tunneling rate of dirac electron in graphene

The usual choice of an orthogonal set of four plane-wave solutions of the free-particle Dirac equation does not lend itself readily to direct and complete physical interpretation except in low energy approximation. A different choice of solutions can be made which yields a direct physical interpretation at all energies. Besides the separation of positive and negative energy states there is a further separation of states for which the spin is respectively parallel or anti-parallel to the direction of the momentum vector. This can be obtained from the Maxwell's equation without charges and current in the $E \parallel H$ configuration. Dirac's four-component equation for the relativistic electron is [5-7]. (see our chapter "Chiral Transverse Electromagnetic standing waves with $E \parallel H$ in the Dirac Equation and the spectra of the Hydrogen Atom", section 2, Intech 2011, Behaviour of electromagnetic waves in different media and structures, edited by Ali Akdagli). Here we consider a bidimensional graphene system so the Dirac's four-component equation for the relativistic electron is:

$$i\hbar \frac{\partial}{\partial t} \psi = \hat{H}^D \psi \quad (45)$$

where:

$$\hat{H}^D = v_F (\vec{\alpha} \cdot \hat{p}) + m v_F^2 \beta \quad (46)$$

$$\alpha_k = \begin{pmatrix} 0 & \sigma_k \\ \sigma_k & 0 \end{pmatrix}, \quad k=1, 2, 3, \quad (47)$$

$$\beta = \begin{pmatrix} I & 0 \\ 0 & -I \end{pmatrix} = \sigma_z \quad (48)$$

and I is the two-by-two identity matrix and the Fermi velocity v_F is deduced from the chiral electrodynamics with $v_F = c(1 \pm k_0 T)$, where T is the chiral parameter in a metamaterial condition. This result is capital to our approach because we find a contact point between the graphene system and optical metamaterial making $v_F = c(1 \pm k_0 T)$, not making $c \rightarrow v_F$ as other authors do it. In Figure 5 we have $1.0073 > k_0 T > 0.9927$.

The Hamiltonian commutes with the momentum vector \hat{p} . In order to resolve this degeneracy we seek a dynamical variable which commutes with both H and \hat{p} . Such a variable is $\hat{\sigma} \cdot \hat{p}$, where $\hat{\sigma}$ is the matrix Pauli. The eigenfunctions of the commuting variables p and $\hat{\sigma} \cdot \hat{p}$ are simultaneous:

$$(\hat{\sigma} \cdot \hat{p})^2 = p^2 \quad (49)$$

Thus for a simultaneous eigenstate of \hat{p} and $\hat{\sigma} \cdot \hat{p}$, the value of $\hat{\sigma} \cdot \hat{p}$ will be $+p$ or $-p$, corresponding to states for which the spin is parallel or antiparallel, respectively, to the momentum vector like a graphene system.

A simultaneous eigenfunction of H and p will have the form of a plane wave

$$\psi_j = u_j \exp[i(\mathbf{p} \cdot \mathbf{r} - Et)/\hbar], \quad j=1, 2, 3, 4 \quad (50)$$

where the ψ_j are the four components of the state function and u_j four numbers to be determined. Then E can have either of the two values.

$$E = \pm \varepsilon = \pm (m^2 v_F^4 + v_F^2 p^2)^{\frac{1}{2}} \quad (51)$$

We now demand that ψ_j be also an eigenfunction of $\hat{\sigma} \cdot \hat{p}$ belonging to one of the eigenvalues p_E , say, where $p_E = \pm p$.

The eigenvalue equation is

$$\hat{\sigma} \cdot \hat{p} \psi = p_E \psi \quad (52)$$

Since W can be given either of the two values $\pm \varepsilon$ and p_E , the two values $\pm p$, we have found for given p four linearly independent plane wave solutions. It is easily verified that they are mutually orthogonal.

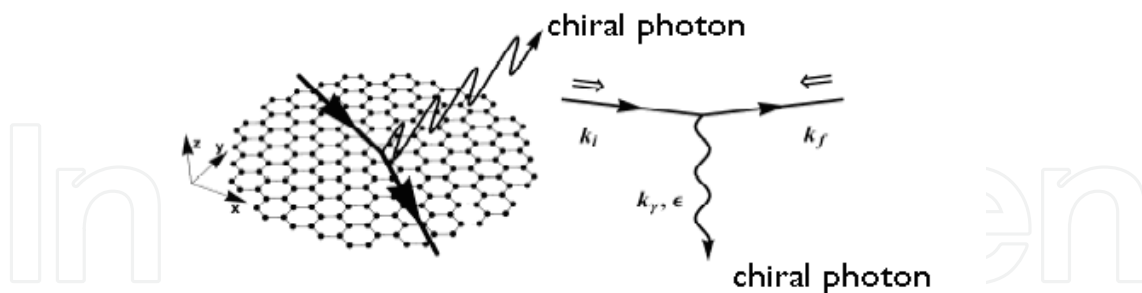


Figure 5. Diagram where the graphene is located in the plane (x, y) , the chiral photon is in either direction. The pontos black figure on the left indicates the position of carbon atoms.

The physical interpretation of the solutions is now clear. Each solution represents a homogeneous beam of particles of definite momentum p , of definite energy, either $\pm \varepsilon$, and with the spin polarized either parallel or antiparallel to the direction of propagation. From here we can obtain the well known equation for graphene $H_0 = -i\hbar v_F \sigma \cdot \nabla$.

In this section, we study the tunneling rate of Dirac electrons in graphene through a barrier with an intense electromagnetic field. A one transport phenomenon in graphene is the chiral tunneling [1, 2, 17, 18]. In mono layer graphene a perfect transmission through a potential barrier in the normal direction is expected. This tunneling effect is due to the chirality of the Dirac electrons, which prevents backscattering in general. This kind of reflectionless transmission is independent of the strength of the potential, which limits the development of graphene-based field-effect transistors (FET). The perfect transmission can be suppressed effectively when the chiral symmetry of the Dirac electrons is broken by a laser field, when the n-p junctions in graphene are irradiated by an electromagnetic field in the resonant condition [19,20]. We consider a rectangular potential barrier with height H_0 , width D in the X direction, and infinite length in the Y direction. The Fermi level lies in the valence band in the barrier region and in the conduction band outside the barrier. The gray filled areas indicate the occupied states. The optical field under chiral condition is propagated perpendicular to the layers surface and it is circularly polarized along the Z, Y direction with a detuning $\Delta_0 = 2E_b - \hbar\omega$. We choose $\Delta_0 > 0$ to ensure that there is no inter-band absorption inside the barrier. Meanwhile, $2E_k \gg \hbar\omega$ is used to guarantee that the influence of the optical field outside the barrier can be neglected. Thus, neglecting the scattering between different valleys, the scattering process of Dirac electrons in K point is described by the time-dependent Dirac equation, Eq. (45) with $m=0$, so $\psi = \psi_g = (\psi_E, \psi_H)^t$ where t means transposed wave function.

$$i\hbar \frac{\partial}{\partial t} \psi_g(r, t) = [H_e + H_0 I + H_{\text{int}}] \psi_g(r, t) \quad (53)$$

where $\psi_g(r, t) = [\phi_A(r, t), \phi_B(r, t)]^t$ is the wave function, $H_e = v_F \hat{\sigma} \cdot p = -i\hbar v_F \hat{\sigma} \cdot \nabla$ is the unperturbed Dirac Hamiltonian obtained from the chiral electrodynamics [17], $\hat{\sigma} = (\sigma_x, \sigma_y)$ are the Pauli matrices, $v_F \approx 10^6 \text{ms}^{-1}$ is the Fermi velocity, $H_0(r)$ is the height of the potential barrier, I is the unit matrix, and H_{int} is the interaction Hamiltonian with a chiral electromagnetic potential.

$$H_{\text{int}} = -\hbar e v_F [\hat{\sigma} \cdot \mathbf{A}] = \hbar \begin{pmatrix} 0 & H_{12} \\ H_{21} & 0 \end{pmatrix} \quad (54)$$

where e is the electron charge and the chiral potential vector is $[\mathbf{A}] = [A_x e^{i\omega t}, iA_y e^{i\omega t}]$ with $i = \sqrt{-1}$ and $|A_x| = |A_y|$ so we have circular polarized wave of the electromagnetic field. When the Dirac electrons perpendicularly collide with the barrier perpendicularly, we can rewrite Eq. (53) as a set of partial differential equations

$$i\hbar \frac{\partial}{\partial t} \phi_A(x, t) = -i v_F \frac{\partial}{\partial x} \phi_B(x, t) + V_0 \phi_A(x, t) + H_{12}(t) \phi_B(x, t) \quad (55)$$

$$i\hbar \frac{\partial}{\partial t} \phi_B(x, t) = -i v_F \frac{\partial}{\partial x} \phi_A(x, t) + V_0 \phi_B(x, t) + H_{21}(t) \phi_A(x, t) \quad (56)$$

Since the tunneling time is of order of sub-picosecond and the potential $H_{12}(t)$ and $H_{21}(t)$ vary as fast as the frequency of incident light beams, this scattering process is strongly time-dependent.

In order to study such a strongly time-dependent scattering process, we employ the finite-difference time-domain (FDTD) method to solve Eq. (47) and Eq. (48) numerically in the time-domain [21]. In the traditional FDTD method, the Maxwell's equations are discretized by using central-difference approximations of the space and time partial derivatives. As a time-domain technique, the FDTD method can demonstrate the propagation of electromagnetic fields through a model in real time. Similar to the discretization of Maxwell's equations in FDTD, we denote a grid point of the space and time as $(i, k) = (i\Delta x, k\Delta t)$ [22]. For the nodal variables we can apply the usual Lee discretization method in 2-D systems with $k_0^2 T^2 \sim 1$ (See Figure 6).

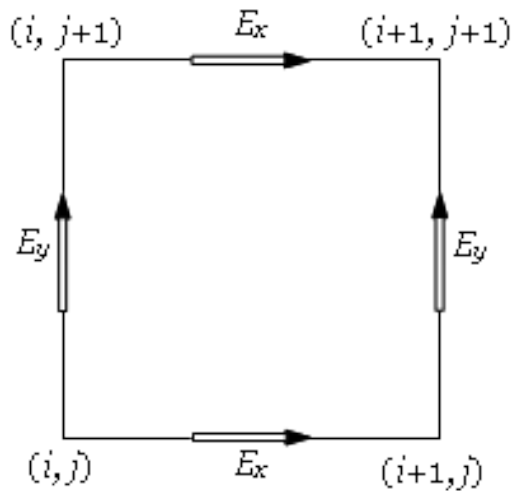


Figure 6. Lee discretization. Here $H_x = (\nabla \times \vec{A})_x E_x = -(\partial(1 + T \nabla \times) \vec{A} / \partial t)_x$ and with $\vec{J} = 0$ (See [21, 22, 24]).

For any function of space and time $G(i\Delta x, k\Delta t) = G^k(i)$, the first order in time or space partial differential can be expressed as:

$$\left(\frac{\partial}{\partial x} G(x, t)\right)_{x=i\Delta x} \approx \frac{G^k(i+1/2) - G^k(i-1/2)}{\Delta x}, \dots, \left(\frac{\partial}{\partial t} G(x, t)\right)_{t=k\Delta t} \approx \frac{G^{(k+1/2)}(i) - G^{(k-1/2)}(i)}{\Delta t}$$

These eqs. can be replaced by a finite set of finite differential equations like:

$$\begin{aligned} \phi_A^{k+1/2}(i) \left[\frac{1}{\Delta t} - \frac{H_0(i)}{2i} \right] &= \left[\frac{1}{\Delta t} + \frac{H_0(i)}{2i} \right] \phi_A^{k-1/2}(i) \\ &- \left[\frac{v_F}{\Delta x} - \frac{H_{12}^k(i+1/2)}{2i} \right] \phi_B^k(i+1/2) \\ &+ \left[\frac{v_F}{\Delta x} + \frac{H_{12}^k(i-1/2)}{2i} \right] \phi_B^k(i-1/2) \end{aligned} \tag{57}$$

For computational stability, the space increment and the time increment need to satisfy the relation $\Delta x > v_F \Delta t$ [21]. Furthermore, the space increment Δx must be far smaller than the wavelength of electrons $\Delta x < \lambda_e / 10$, and the time increment must be far smaller than the period of the electromagnetic field T_l .

At the boundary, one-dimensional Mur absorbing boundary conditions are used [21-22]. To compare our results with [25] which use linear polarization for the vector potential A where the chiral parameter T is zero, we consider at the input boundary, a normalized Gaussian electronic wave packet, where t_g and τ_g denote the peak position and the pulse width, respectively. Thus, by solving Eq. (57) directly in the time domain we can demonstrate the propagation of a wave packet through a barrier in real time.

Numerical simulations are shown in Fig. 7. The following parameters are used in our calculation: the peak position $t_0 = 1.5$ ps, the pulse width $\tau_g = 1.0$ ps, the space increment $\Delta x = 0.1$ nm, the time increments $\Delta t = 5 \times 10^{-5}$ ps, and the height of the potential barrier $H_0 = 500$ meV.

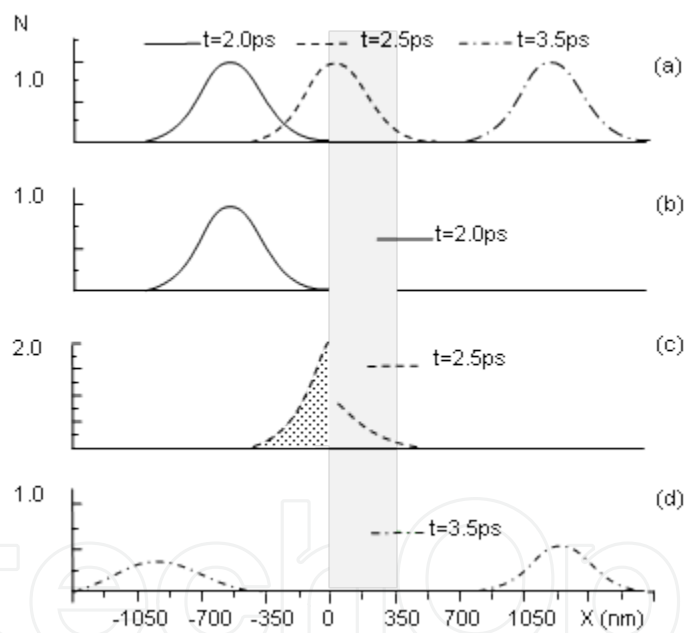


Figure 7. a) Numerical simulations of a wave packet given by $N = |A|^2 + |B|^2$, tunneling through a barrier without pump beams. Figures (b)-(d) show the time sequence of a wave packet tunneling through a barrier with pump intensity $I_\omega = 3 \text{ MW} / \text{cm}^2$, $\Delta_0 = 5 \text{ meV}$, and $D = 350$ nm. The light grey shows the barrier area.

When there is no pump beams, a perfect chiral tunneling can be found [see Fig. 7 (a)]. This result is consistent with that of Ling et al. [25]. But when the sample is irradiated by an intense non resonant laser beam, a reflected wave packet appears [see Fig. 7 (d)]. The perfect transmission is suppressed. By analyzing the transmitted wave packet and the reflected wave packet, we can obtain the tunneling rate.

To explain the suppression of chiral tunneling, we first investigate the chiral potential wave in the barrier within a rotating wave approximation [23, 24]. Figure 7 (a) shows the renormalized band as a function of momentum k with intensity $I_\omega = 3\text{MW}/\text{cm}^2$.

Here, the important point is that we make $\pm k_0 T \sim 1 + \alpha \approx 1.0073$, where $\alpha = e^2 / (4\pi\epsilon_0 \hbar c)$ is the fine structure constant, so we verify that our chiral theory is correct. Without external beams, (fig. 7 (a)), we verify the known results on chiral tunneling [11]. Figures 7 (b)-(d) show the time sequence of a wave packet tunneling through a barrier with pump intensity $I_\omega = 3\text{MW}/\text{cm}^2$, $\Delta_0 = 5\text{meV}$, and $D = 350\text{nm}$.

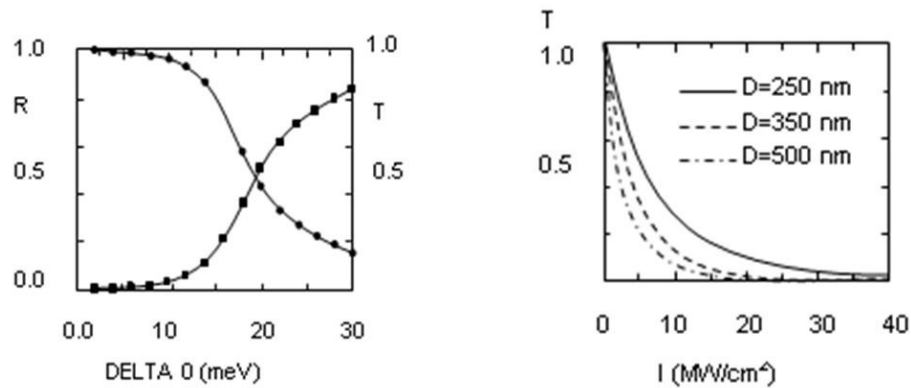


Figure 8. Left: The reflectance R(circles) and the transmittance T (squares) of the barrier as a function of the detuning for $I_\omega = 3\text{MW}/\text{cm}^2$ and $D = 350\text{nm}$. Right: The transmittance versus $I_\omega (\text{MW}/\text{cm}^2)$, having D as parameter. Here, $k_0^2 T^2 \approx 1$, that is the wave electric field is almost parallel to the wave magnetic field within the graphene device.

Under intense light beams, the dressed states are strongly mixed with valence states and conduction states. Therefore, the chiral symmetry of Dirac electrons in graphene can be broken and perfect chiral tunneling is strongly suppressed. Numerical results are shown in Fig. 8 (left) with pump intensity $I_\omega = 3\text{MW}/\text{cm}^2$ and $D = 350\text{nm}$. From Fig. 8(left) we can find that the transmission is strongly suppressed, even with laser detuning (e.g., $\Delta_0 = 10\text{meV}$, the transmittance is about 0.03).

Figure 8 (left), show that the reflectance decreases, and the transmittance increases as Δ_0 increases. The strong laser field can enhance band mixing and reduce the transmittance. If D increases we can see that the wide barrier can prolong the interaction time between electrons and photons, reduce the tunneling rate, and lower the threshold of the pump laser power (Figure 8 right). Our results can be compared with [25] which use linear polarization of H_{int} however we think that inside of a plate of graphene, the eigenvectors of A have to be characterized as chiral waves, because the electrons have a chiral nature in a graphene device. Is for this reason that our numerical results correspond to half times the results shown in [25].

5. Zitterbewegung of optical pulses near the Dirac point inside a negative-zero-positive index metamaterial

This optical analog of the *Zitterbewegung* effect is similar to two-dimensional (2DPC) photonic crystal.

The *Zitterbewegung* effect can appear in solids, because the electron at the touching point between two interacting bands in a solid also obeys the massless Dirac equation [26]. In recent years, a growing attention has been devoted to the simulations or demonstrations of the *Zitterbewegung* effects in controllable physical systems, such as, ultra cold atoms, superconductors, semiconductor nanostructures with spin-orbit coupling, a single trapped ion, and graphene.

For a homogenous medium, when a light field is polarized in the z direction, the Beltrami's equation $\nabla \times \vec{E}^\pm(\vec{r}, t) = \mp k_\pm \vec{E}^\pm$ can be transformed as a Helmholtz equation written as

$$\left(\frac{\partial}{\partial x} + i\frac{\partial}{\partial y}\right)\left(\frac{\partial}{\partial x} - i\frac{\partial}{\partial y}\right)E_z(x, y, \omega) = (ik(\omega))^2 E_z(x, y, \omega) \quad (58)$$

with a wave number $k(\omega)$. This equation can be written in the form of the Dirac equation

$$\begin{pmatrix} 0 & -i\left(\frac{\partial}{\partial x} - i\frac{\partial}{\partial y}\right) \\ -i\left(\frac{\partial}{\partial x} + i\frac{\partial}{\partial y}\right) & 0 \end{pmatrix} \begin{pmatrix} E_{z1}(x, y, \omega) \\ E_{z2}(x, y, \omega) \end{pmatrix} = k(\omega) \begin{pmatrix} E_{z1}(x, y, \omega) \\ E_{z2}(x, y, \omega) \end{pmatrix} \quad (59)$$

In the case of graphene near of $\epsilon_{\parallel}/\epsilon_p, \mu_{\parallel}/\mu_p \approx 0$, there are two bands touch each other forming a double-cone structure with a linear dispersion, which can also be called Dirac Point. Near the Dirac point the light transport obeys the massless Dirac equation if we make $v_F = c(1 \pm k_0 T) = v_D$. Also naturally, it would be of great interest to find out what is the condition to have the Dirac dispersion for the light field in a homogenous medium, the wave vector of a medium, $k(\omega)$, can be expanded as $k(\omega) = k(\omega_D) + (\omega - \omega_D)/v_D + \dots$ so if $k(\omega_D) = 0$, then we have a linear dispersion $k(\omega) = (\omega - \omega_D)/v_D$, and the Dirac equation is

$$\begin{pmatrix} 0 & -iv_D\left(\frac{\partial}{\partial x} - i\frac{\partial}{\partial y}\right) \\ -iv_D\left(\frac{\partial}{\partial x} + i\frac{\partial}{\partial y}\right) & 0 \end{pmatrix} \begin{pmatrix} E_{z1}(x, y, \omega) \\ E_{z2}(x, y, \omega) \end{pmatrix} = (\omega - \omega_D) \begin{pmatrix} E_{z1}(x, y, \omega) \\ E_{z2}(x, y, \omega) \end{pmatrix} \quad (60)$$

where $E_{z1}(x, y, \omega), E_{z2}(x, y, \omega)$ are two eigenfunctions of the electrical fields (polarized in the z -direction) corresponding to the same frequency ω , and v_D is the group velocity at the Dirac point (ω_D). For media satisfying Eq. (58) with $\omega_D > 0$, the wave number, $k(\omega)$, varies from negative to zero and then to positive with the frequency, and so does the refractive index of the medium with zero refractive index at ω_D .

Note that the positive and negative branches of the band structure coexist. Equation (58) is the massless Dirac equation of the light fields in homogenous materials, which is the same as that of electrons in graphene [27]. Therefore, for the NZPI metamaterial [satisfying Eq. (58)], we will have the Dirac point with a double-cone structure for the light field at frequency ω_D . It is expected that the propagation of the light field is analogous to that of the electron in graphene. In fact, in the 2DPC [28], the effective refractive index varies from negative to positive near this Dirac point. At ω_D , Eq. (45) takes the form of diffusion equation,

$$-iv_D(\frac{\partial}{\partial x} - i\frac{\partial}{\partial y})E_{z1}(x, y, \omega) = 0, \quad -iv_D(\frac{\partial}{\partial x} + i\frac{\partial}{\partial y})E_{z2}(x, y, \omega) = 0 \quad (60)$$

which are the same as that of the massless Dirac equation at zero energy. [29]. Therefore, it can be predicted that the behavior of light fields at ω_D has the diffusive properties inside the medium of Eq. (2), like electrons at Dirac point of graphene [27-29]. At or near ω_D , because of $k^2 = k_x^2 + k_y^2 \approx 0$, the k_y component becomes a pure imaginary number for any real k_x , thus the fields along the y direction between a given interval L have the total energy transmittance

$$T_{all} = \int_{-\infty}^{\infty} (\exp(-|k_x|L))^2 dk_x = 1/L \quad (61)$$

which tells us that the propagation of light field at (or near) ω_D exhibits the $L / 1$ scaling, a main characteristic of the diffusion phenomenon. This effect can be obtained if $\epsilon_{||} / \epsilon_p, \mu_{||} / \mu_p \rightarrow 0$ with low damping rates.

Here, the Dirac point with the double-cone structure for the light field can also be realized in a homogenous negative-zero-positive index (NZPI) medium [26], in which the two-dimensional Helmholtz equation could be written as the two-dimensional massless Dirac equation. The condition for the realization of the Dirac point in the homogenous optical medium is the index varying from negative to zero and then to positive with frequency, and the light field also obeys eq. (45) near the Dirac point. Thus, in this work, we show that the *Zitterbewegung* effect with optical pulses appears near the Dirac point in NZPIM slabs. With the realization of the NZPIMs in experiments, we believe that it already has a great possibility to observe *Zitterbewegung* effect with optical pulses in the GHz region.

6. Theoretical description of minimal conductivity in graphene under chiral approach

The first results on the theoretical combination of graphene electron transport properties and a characteristic property of Dirac chiral fermions were obtained by Katsnelson et al, [2]. The intrinsic nature of Dirac fermions gives rise to minimal conductivity even for an ideal crystal, that is, without any scattering processes. The simplest way for the theoretical con-

sideration is the Landauer approach [29]. Assuming that the sample is a ring of length L_y in y direction; author used the Landauer formula to calculate the conductance in the x direction (Fig. 9).

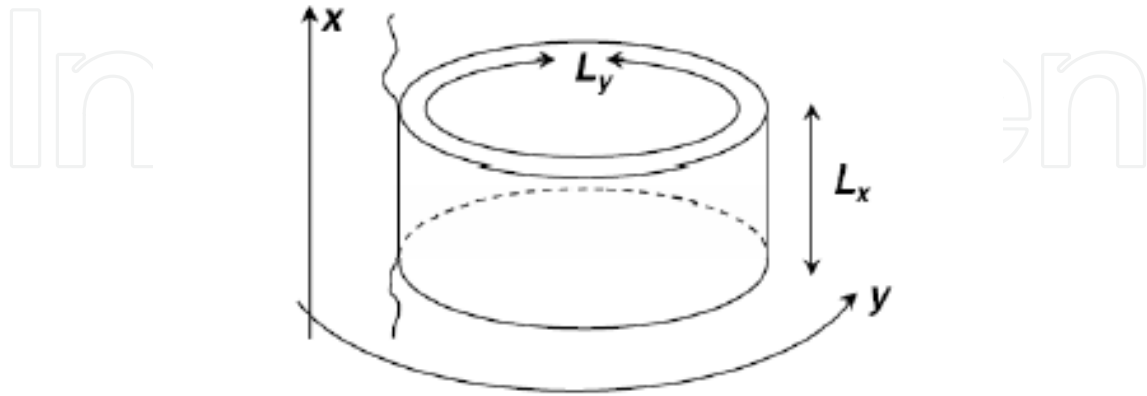


Figure 9. Geometry of the sample. The direction of the current is parallel to the x axis [27].

The convenient boundary conditions are not physical, but to get finite transparency one should choose $L_x L_y$.

In the coordinate representation the Dirac equation (59) at zero energy takes the form ($\Psi_i = v_D E_{zi}$)

$$-i\left(\frac{\partial}{\partial x} - i\frac{\partial}{\partial y}\right)v_D E_{z1}(x, y, \omega) = -i\left(\frac{\partial}{\partial x} - i\frac{\partial}{\partial y}\right)\Psi_1 = 0 \quad (62)$$

$$-i\left(\frac{\partial}{\partial x} + i\frac{\partial}{\partial y}\right)v_D E_{z2}(x, y, \omega) = -i\left(\frac{\partial}{\partial x} + i\frac{\partial}{\partial y}\right)\Psi_2 = 0 \quad (63)$$

The solutions of these equations are $\Psi_1(x - iy), \Psi_2(x + iy)$, which are complex conjugated functions which are general solutions.

Due to periodicity in y direction both wave functions should be proportional to $\exp(ik_y y)$ where $k_y = 2\pi n / L_y$, $n = 0, \pm 1, \pm 2, \dots$. This means that the dependence on the x is also fixed:

the wave functions are proportional to $\exp(2\pi n x / L_y)$. The introduced boundary conditions at the sample edges are $x=0$ and $x=L_x$. The assumption is that the sample is doped graphene with the Fermi energy $E_F = v k_F = -V_0$. The wave functions in the sample are supposed to have the same y -dependence, that is, $\Psi_{1,2}(x, y) = \Psi_{1,2}(x) \exp(ik_y y)$.

Requiring continuity of the each wave function at the edges of sample, one can find the transmission coefficient:

$$T_n = \frac{\cos^2\phi}{\cosh^2(k_y L_x) \cdot \sin^2\phi} \quad (64)$$

Where $\sin\phi = k_y / k_F$,

$$k_x = \sqrt{k^2 - k_y^2} \quad (74)$$

Further, one should assume that $k_F L_x \gg 1$ and put $\phi = 0$ in equation. Thus, the trace of the transparency which is just the conductance per valley per spin is

$$g = \frac{e^2}{h} \text{tr}(\sum T_n) = \frac{e^2}{h} \left(\sum_{n=-\infty}^{\infty} \frac{1}{\cosh^2(k_y L_x)} \right) = \frac{e^2}{h} \frac{L_y}{\pi L_x} \quad (65)$$

The conductance then equals $\sigma L_y / L_x$ and the conductivity is $e^2 / \pi h$. Experimentally, it is close to e^2 / h [31], that is in π times larger than present estimation.

Zitterbewegung – circular motion of elementary particles caused by an interference between positive and negative energy states – leads to the fluctuation of the position of an electron. This relativistic “jittering” of an electron in graphene could be interpreted in terms of classical physics as an interaction of electron with some potential caused by the presence of disorder in crystal. Therefore, the Zitterbewegung plays a role of “intrinsic” disorder in the system which appears in the presence of minimal conductivity of the ideal crystal (without scattering) even at zero temperatures.

Under this chiral approach, we show that the optical transparency of suspended graphene can be defined by the fine structure constant, $\alpha = e^2 / \hbar c$, the parameter that describes coupling between light and relativistic electrons and is traditionally associated with quantum electrodynamics rather than condensed matter physics. Despite being only one atom thick, graphene is found to absorb a significant ($\alpha = 0.78\%$ to $\pi\alpha = 2.3\%$) fraction of incident white light, which is a consequence of graphene’s unique electronic structure. This value translates directly into universal dynamic conductivity $G = e^2 / 4\pi\hbar$ within a few % accuracy.

There is a small group of phenomena in condensed matter physics, which are defined only by the fundamental constants and do not depend on material parameters. Examples are the resistivity quantum h / e^2 that appears in a variety of transport experiments, including the quantum Hall effect and universal conductance fluctuations, and the magnetic flux quantum h / e playing an important role in the physics of superconductivity (here h is the Planck constant and e the elementary charge). By and large, it requires sophisticated facilities and special measurement conditions to observe any of these phenomena. Here, we show that such a simple observable as the visible transparency of graphene [1] is defined by the fine structure constant, α . Our results are in agreement with the theory of ideal two-dimensional (2D) Dirac fermions [2,3] and its recent extension into visible optics [4], which takes into ac-

count the triangular warping and nonlinearity of graphene's electronic spectrum, but our result is π^{-1} times the result of [2,3].

Optical properties of thin films are commonly described in terms of dynamic or optical conductivity G . For a 2D Dirac spectrum with a conical dispersion relation $\varepsilon = \hbar v_F |k|$ (k the wavevector). G was theoretically predicted [32, 33] to exhibit a universal value $G = e^2 / 4\hbar$, our result is $G_0 = e^2 / 4\pi\hbar$ if the photon energy E is much larger than both temperature and Fermi energy ε_F . Both conditions are stringently satisfied in our visible-optics experiments. The universal value of G also implies that all optical properties of graphene (its transmittance T , absorption A_{abs} and reflection R) can be expressed through fundamental constants only (T , A_{abs} and R are unequivocally related to G in the 2D case). In particular, it was noted by Kuzmenko *et al* [34] that $T_{transp} = (1 + 2\pi G_0 / c)^{-2} \approx (1 + 0.5\pi\alpha)^{-2} \approx 1 - \pi\alpha$ for the normal light incidence. Our result is given by $T_{transp} \approx 1 - \alpha$. We emphasize that – unlike G – both T and R are observable quantities that can be measured directly by using graphene membranes.

7. Absorption of light by quasi 2D Dirac fermions

Here, following [35], we show how the universal value of graphene's opacity can be understood qualitatively, without calculating its dynamic conductivity. Let a light wave with electric field E and frequency ω fall perpendicular to a graphene sheet of a unit area. The incident energy flux is given by $W_i = c / 4\pi (|E|^2)$

Taking into account the momentum conservation k for the initial $|i\rangle$ and final $|f\rangle$ states, only the excitation processes pictured in Fig. 10 contribute to the light absorption. The absorbed energy $W_a = n\hbar\omega$ is given by the number n of such absorption events per unit time and can be calculated by using Fermi's golden rule as $n = (2\pi / \hbar) (|L|^2) D$ where L is the matrix element for the interaction between light and Dirac fermions, and D is the density of states at $\varepsilon = E / 2 = \hbar\omega / 2$ (see Fig. A1). For quasi 2D Dirac fermions, $D(\hbar\omega / 2) = \hbar\omega / \pi\hbar^2 v_F^2$ and is a linear function of ε .

The interaction between light and Dirac fermions is generally described by the Hamiltonian $H = v_F \hat{\sigma} \cdot \hat{p} = v_F \hat{\sigma} \cdot (\hat{p} - e/cA) = H_0 + H_A$

where the first term is the standard Hamiltonian for 2D Dirac quasiparticles in graphene [1] and

$H_A = -v_F \hat{\sigma} \cdot (e/c)A = v_F \hat{\sigma} \cdot (e/i\omega)E$ describes their interaction with electromagnetic field.

Here $A = (ic/\omega)E$ is the vector potential and σ the standard Pauli matrices. Averaging over all initial and final states and taking into account the valley degeneracy, our calculations yield

$$L^2 = |\langle f | v_F \hat{\sigma} \cdot (e/i\omega)E | i \rangle|^2 = (1/8)e^2 v_F^2 E^2 / \omega^2$$

This results in $W_a = (e^2/4\hbar) |E|^2$ and, consequently, absorption $A_{abs} = W_a/W_i = \pi e^2/c\hbar = \pi\alpha$ both of which are independent of the material parameter v_F that cancels out in the calculations of W_a . Also note that the dynamic conductivity $G = W_a/|E|^2$ is equal to $e^2/4\hbar$. Our result is $A_{abs} \approx W_a/W_i = \pi e^2/\pi c\hbar = \alpha$ in correspondence with $v_F = c(1 - k_0T)$. Because graphene practically does not reflect light ($R \ll 1$ as discussed above), its opacity ($1 - T$) is dominated by the derived expression for A_{abs} .

In the case of a zero-gap semiconductor with a parabolic spectrum (e.g., bilayer graphene at low ϵ), the same analysis based on Fermi's golden rule yields $A_{abs} = 2\pi\alpha$. This shows that the fact that the optical properties of graphene are defined by the fundamental constants is related to its 2D nature and zero energy gap and does not directly involve the chiral properties of Dirac fermions.

On a more general note, graphene's Hamiltonian H has the same structure as for relativistic electrons (except for coefficient v_F instead of the speed of light c). The interaction of light with relativistic particles is described by a coupling constant, a.k.a. the fine structure constant. The Fermi velocity is only a prefactor for both Hamiltonians H_0 and H_A and, accordingly, one can expect that the coefficient may not change the strength of the interaction, as indeed our calculations show.

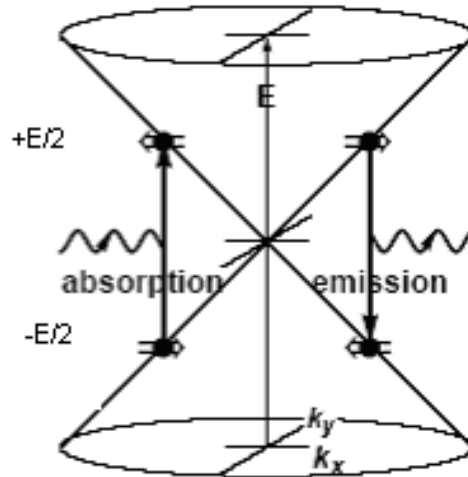


Figure 10. Excitation processes responsible for absorption of light in graphene.

Thus, we have found that the visible opacity of suspended graphene is given by $\pi\alpha$ within a few percent accuracy and increases proportionally to the number of layers N for few-layer graphene. Its dynamic conductivity at visible frequencies is remarkably close to the universal value of $(e^2/4\hbar)N$. The agreement between the experiment and theory is particularly striking because it was believed the universality could hold only for low energies ($< 1\text{eV}$)

beyond which the electronic spectrum of graphene becomes strongly warped and nonlinear and the approximation of Dirac fermions breaks down.

Electrons from the valence band (bottom) are excited into empty states in the conduction band with conserving their momentum and gaining the energy $E = \hbar \omega$.

The approximation of 2D Dirac fermions is valid for graphene only close to the Dirac point and, for higher energies ϵ , one has to take into account such effects in graphene's band structure as triangular warping and nonlinearity.

Most theories suggest $4e^2/\pi h$, which is about π times smaller than the typical values observed experimentally. The reason of disagreement is still an open question – “mystery of a missing pie”. A value of conductivity $\sim e^2/h$ at the Dirac point can emerge in case of preservation of chiral symmetry by disorder or when the dominant disorder does not scatter electrons between two valleys. Furthermore, macroscopic inhomogeneity (on the scale larger than the mean free path) is also important for measurements of σ_{\min} .

8. Conclusions

In this chapter we presented a short review on the chiral propagation of electron waves in monolayer graphene and optical simulation with optical field in the negative-zero-positive index metamaterial NZPIM and its close connection. Section II presented an enhanced vector diagram of Maxwell's equations for chiral media with quasi parallel electromagnetic fields, $E \parallel H$. Chiral waves in graphene acting as metamaterial media were discussed in section III. In section IV, two equations and tunneling rate of Dirac electron in graphene were derived. In Section V, *Zitterbewegung* of optical pulses near the Dirac point inside a negative-zero-positive index metamaterial, showed that the chiral field near the Dirac point becomes a diffusive wave. The last sections described the theoretical description of minimal conductivity in graphene under chiral approach and absorption of light by quasi 2D Dirac fermions.

We reviewed the formulation of graphene's massless Dirac Hamiltonian, under the chiral electromagnetism approach, like a metamaterial medium, hopefully demystifying the material's unusual chiral, relativistic, effective theory. The novel result here was that in our theory we did not make $c \rightarrow v_F$ [1, 2, 27-35], but we obtained v_F as $v_F = c(1 - k_0 T)$ if $k_0 T > 0$ or $v_F = c(1 + k_0 T)$ if $k_0 T < 0$. These results were derived of the Chiral Electrodynamics with T as the chiral parameter and $k_0 = \omega/c$ [5, 6, 7]. This situation corresponds to chiral electrons where the E field is almost parallel to the H field, and the movement of electron is helical in the valence band of the membrane graphene. Semi classically, for an electron in hydrogen atom, this condition was shown by Huang (2006) for E wave perpendicular to H wave with radiation ($E = H$) and by Torres-Silva for E parallel to H , without radiation ($E = iH$), see refs ([5, 36, 37]). Here, we have extended this result to the electron bound to a carbon atom.

There is a small group of phenomena in condensed matter physics, which are defined only by the fundamental constants and do not depend on material parameters. Examples are the

resistivity quantum h/e^2 that appears in a variety of transport experiments, including the quantum Hall effect and universal conductance fluctuations, and the magnetic flux quantum h/e playing an important role in the physics of superconductivity. In this chapter we founded that under this chiral approach, the optical transparency of suspended graphene can be defined by the fine structure constant, $\alpha = e^2/\hbar c$, that is $T_{trasp} \approx 1 - \alpha$, and $v_F/c = \alpha = (1 - k_0 T)$.

Also we give a support to the similitude of the band structure of a macroscopic photonic crystal with the electronic band structure of graphene, which is experimentally much more difficult to access, allows the experimental study of various relativistic phenomena. With our analytical and numerical analysis we hope to verify that, similar behaviors exist to electrons in graphene treated as mass-less particle, ie, electron wave discovered only 8 years ago graphene is already one of the most studied carbon allotropes. But this material still poses a lot of theoretical and experimental questions, which have to be answered.

Acknowledgements

I wish to thank to colleague Jorge Benavides Silva of the EIEE for many useful discussions on particles and photons

Author details

H. Torres-Silva*

Address all correspondence to: htorres@uta.cl

Escuela de Ingeniería Eléctrica y Electrónica Universidad de Tarapacá- Arica, Chile

References

- [1] Novoselov, S., et al. (2005). *Nature*, 438, 197-200.
- [2] Katsnelson, M. I., et al. (2006). *Nature Physics*, 2, 620-624.
- [3] Wilton, D. (1995). *IEEE Antennas and Propagation Magazine.*, 37, 7-11.
- [4] Uckun, S. (1998). *Electrotechnical Conference. Melecon 98*, 283-286.
- [5] Torres-Silva, H. (2011). Chiral Transverse Electromagnetic standing waves with $E \parallel H$ in the Dirac Equation and the spectra of the Hydrogen Atom. ", section 2. Intech, vol Behavior of electromagnetic waves in different media and structures, edited by Ali Akdagli

- [6] Torres-Silva, H. (2000). Internal publication on Chiral Electrodynamics. (in spanish), PCI:00.1036/97 UTA-CHILE
- [7] Torres-Silva, H. (2008). *Ingeniare*, 16(1), pp. 43-47, 48-52.
- [8] Shelby, R. A., et al. (2001). *Science* [5514], 292, 77-79.
- [9] Veselago, V. G. (1968). *Soviet Physics Uspekhi*, 10(4), 509-514.
- [10] Smith, D. R., et al. (2000). *Phys. Rev. Lett*, 84(18), 4184-4187.
- [11] Monzon, C., & Forester, D.W. (2005). *Phys. Rev. Lett*, 95, 123904.
- [12] Torres-Silva, H. (2008). *Ingeniare*, 16, 119-122.
- [13] Lindell, I., Sihvola, A. H., Tretyakov, S. A., & Viitanen, y. A. J. (1994). *Electromagnetic Waves in Chiral and Bi-Isotropic Media*. Artech House, Boston.
- [14] Plum, E., Zhou, J., Dong, J., Fedotov, V. A., Koschny, T., Soukolis, C. M., & Zheledev, y. N. I. (2009). *Physical Review B*, 79(3), 0354071-0354076.
- [15] Tretyakov, S., Nefedov, I., Sihvola, A., Maslovski, S., & Simovski, C. (2003). *J. Electromagn. Waves Appl*, 17, 695.
- [16] Zhou, J., Dong, J., Wang, B., Koschny, T., Kafesaki, M., & Soukoulis, C. (2009). *Phys. Rev. B*, 79, 121104.
- [17] Hannes, W. R., & Titov, M. (2010). *Europhysics Letters*, 89, 47007.
- [18] Abanin, D. A., & Levitov, L. S. (2007). *Science*, 317, 641.
- [19] Elias, D. C., et al. (2009). *Science*, 323, 610.
- [20] Fistul, M. V., & Efetov, K. B. (2007). *Phys. Rev. Lett* ., 98, 256803.
- [21] Yee, K. S. (1966). *IEEE Transactions on Antennas and Propagation*, ., 14, 302.
- [22] Mur, G. (1981). *IEEE Transactions on Electromagnetic Compatibility*, EMC-23, 377.
- [23] Fistul, M. V., & Efetov, K. B. (2007). *Phys. Rev. Lett*, 98, 256803.
- [24] Torres-Silva, H. (2011). *Ingeniare*, 19, 67-75.
- [25] Ling, Jiang-Tao, Su, Fu-Hai, Huang, Hai, & Xin, Hai. (2007). Arxiv:1007.3430 , 3
- [26] Wang, Li-Gang, et al. (2009). *Opt. Lett*, 34, 1510-1512.
- [27] Nomura, K., & Mac Donald, A. H. (2007). *Phys. Rev. Lett*, 98, 076602.
- [28] Notomi, M. (2000). *Phys. Rev. B*, 62, 10696.
- [29] Katsnelson, M. I. (2006). *Eur. Phys. J. B*, 51, 157.
- [30] Zhang, F., et al. (2008). *J. Appl. Phys*, 103, 084312.
- [31] Novoselov, K. S., et al. (2005). *Nature*, 438, 197-200.

[32] Gusynin, V. P., et al. (2006). *Phys. Rev. Lett.*, 96, 256802.

[33] Falkovsky, L. A., et al. (2007). *Phys. Rev. B*, 76, 153410.

[34] Kuzmenko, A. B., et al. (2008). *Phys. Rev. Lett.*, 100, 117401.

[35] Nair, R., et al. (2008). *Science*, 320, 1308.

[36] Huang, X. Q. (2006). arxiv:physics/0601169.

[37] Torres-Silva, H. (2008). *Ingeniare*, 16, 24-30.

IntechOpen

